Soft Matter

Cite this: *Soft Matter*, 2011, **7**, 9184

www.rsc.org/softmatter

PAPER

Propensity and geometrical distribution of surface nanobubbles: effect of electrolyte, roughness, pH, and substrate bias

Monalisa Mazumder and Bharat Bhushan*

Received 31st March 2011, Accepted 13th July 2011
DOI: 10.1039/c1sm05560g

Nanobubbles are believed to have surface charges at the gas–liquid interface. However, the effect of various factors on the formation mechanism and stability of these charged species is not well understood. Using atomic force microscopy (AFM) in tapping mode (TMAFM), the propensity of formation and geometrical distribution of nanobubbles on an ultra-thin polystyrene (PS) film immersed in deionized (DI) water and saline (sodium chloride) solution was investigated. The results reveal that in saline solution, nanobubbles form in larger number and size as compared to nanobubbles in DI water. This is attributed to the enhanced surface charge stabilization of the nanobubbles caused by the electrolyte ions in saline solution. A PS film of higher roughness causes the formation of larger nanobubbles due to the presence of more nucleation sites provided by surface asperities, causing numerous nanobubbles in close proximity to coalesce to form larger ones. The study of the effect of pH shows that nanobubbles are more stable in an alkaline solution than in an acidic solution. The results further reveal that the size of nanobubbles increases with increasing positive substrate bias, whereas there is no measurable change in size with increasing negative substrate bias, possibly due to differential charging at the interfaces across the non-conductive PS film.

1. Introduction

The study of the interactions between hydrophobic surfaces and aqueous solutions reveals that during wetting, spherical cap shaped bubbles with sub-100 nm diameter are formed on the hydrophobic surface at the solid–liquid interface. These bubbles with nanoscale dimensions are generally called surface nanobubbles or simply nanobubbles. The nanobubbles are believed to be charged species and an electrical double layer forms at the gas–liquid interface which imparts electrostatic stabilization to these structures. Electrolysis of water into H^+ and OH^- ions provides the surface charges of nanobubbles. If a surface charge is present on the sample surface, the nanobubbles of opposite polarity get attracted to the surface. Nanobubbles are formed readily on water-repellant hydrophobic surfaces. The size and propensity of nanobubbles are potentially controlled by the charge species in the liquid wetting the hydrophobic surface, bias at the surface and surface heterogeneity among others.

The presence of nanobubbles may influence adhesion of hydrophobic surfaces in liquid,[2] fluid flow characteristics in micro/nanochannels,[5,12,30] engineering of micro/nanofluidics based biosensors,[5] adsorption and immobilization of biomolecules,[4] and patterning of nanotextured surfaces.[10] A wide variety of techniques have been employed to detect nanobubbles such as rapid cryofixation/freeze fracture,[26] neutron reflectometry,[25] high-energy X-ray reflectivity,[21] and internal reflection infrared spectroscopy.[38] Atomic force microscopy (AFM) in tapping mode (TMAFM) has emerged as a particularly powerful tool for studying nanobubbles.[30]

In TMAFM, an oscillating tip intermittently contacts the sample surface with much lighter force than in contact mode and thus limits deformation and distortion of the nanobubbles being imaged. Several researchers have tried to image nanobubbles in TMAFM.[1,3,8,33,34,37,39] In TMAFM, nanobubbles formed on a polystyrene (PS) film immersed in deionized (DI) water were shown to coalesce under the influence of scan load and scan speed.[7] Investigation of time evolution of nanobubbles and surface morphology of the PS film revealed the formation of nanoindents due to the pressure exerted by nanobubbles.[31] These nanobubbles are found to be stable and can exist for more than 20 h.[33] Past studies[17] suggest that a nanobubble is a charged species and the resulting electrostatic force between the electrical double layers that form therein is a significant factor determining the stability of nanobubbles. Such electrostatic stabilization is likely to be influenced by ionic constituents of solution and hence dissolved electrolytes in solution among others. Increased electrolyte concentration was shown to affect coalescence of free nanobubbles in solution.[17] In the case of surface nanobubbles forming on a hydrophobic surface immersed in liquid, the results appear to be influenced strongly by system conditions such as surface heterogeneity.[1]

Nanoprobe Laboratory for Bio-& Nanotechnology and Biomimetics (NLB2), The Ohio State University, 201 West 19th Avenue, Columbus, OH, 43210-1142, USA. E-mail: Bhushan.2@osu.edu

Some studies[14,37] showed that the stability or morphology of sparsely populated pre-existing nanobubbles did not change significantly with the concentration of electrolytes such as NaCl. On the other hand, it was argued that the stability of densely populated nanobubbles in close proximity can be affected by electrical double layer force and hence by addition of NaCl.[3] Moreover, being a charged species, it can be conjectured that surface nanobubbles would be affected by the pH of the solution. A combination of laser light scattering and ζ-potential measurements in aqueous solution of water-soluble organic molecules shows that the stability of nanobubbles in solution is strongly influenced by the pH of the solution.[17] The study further shows that similar to macroscopic gas/water interface without solutes,[20,27] nanobubbles in solution are negatively charged with an electrical double-layer. Zhang *et al.*,[37] in contrast, noted insensitivity of the nanobubbles, in terms of stability and morphology, to the addition of salts or solution pH.

A degree of complexity of the subject is emphasized by the observation that surface roughness and chemical heterogeneity can sometimes have a significant influence on the tendency of nanobubble formation on surfaces of comparable hydrophobicity as determined by the water contact angle measurements.[29,32,38] Yang *et al.*[33] showed that larger and fewer nanobubbles formed on rough silanated surfaces than those with a smooth surface of similar hydrophobicity. Nanobubbles also preferentially formed at areas of roughness upon invoking a solvent-exchange method (process of flushing a solvent with higher gas solubility, generally ethanol, and then with a solvent of lower gas solubility such as water through the AFM fluid cell and over the hydrophobic surface) to generate nanobubbles.[39]

The shape of a nanobubble has also been debated. Multitudes of research groups have shown that nanobubbles constitute an array of spherical cap-shaped gaseous domains at the solid–liquid interface.[24,37] However, flat gaseous layers, termed "nanopancakes," have been observed on highly oriented pyrolytic graphite (HOPG) either alone or in conjunction with nanobubbles.[13]

Another interesting phenomenon is the electrolytic generation of nanobubbles by electrolysis of water on a hydrophilic HOPG surface.[34] The coverage and volume of the surface nanobubbles are shown to increase with increasing voltage applied across the electrodes. Electrochemical generation of hydrogen has been reported to induce the formation of nanobubbles at the electrode surface in sulfuric acid solution. The concentration of hydrogen nanobubbles in electrolyzed water was observed to depend on the ionic strength of the solution.[18] These findings point towards the possibility that surface charge might play a pivotal role in the mechanism of formation and stability of nanobubbles. For an in-depth understanding of the interaction of these charged species, it is important to study the influence of substrate bias on the surface nanobubbles. As an example, the surface charge develops on polymeric micro/nanochannels which may affect fluid flow. Such fundamental study would find potential applications in designing of micro/nanochannels,[12] biosensors/biochips,[5,15] and controlled drug delivery[19] among others. However, despite its practical relevance, the effect of a voltage applied between the substrate and the liquid droplet on the characteristics of nanobubbles formed on non-conductive hydrophobic film on substrate has not been reported yet.

A systematic comprehensive study of the influence of electrolyte, surface roughness, pH, and the effect of substrate bias on formation and distribution characteristics of surface nanobubbles is thus crucial for a fundamental understanding of nanobubble characteristics as well as for potential micro/nanofluidics applications. The objective of the present research is to study the effect of electrolyte on the propensity of the formation, geometrical distribution, evolution with time, effect on film surface morphology, and 3D shape of the nanobubbles. The role of surface charge on the stability and geometrical distribution of nanobubbles also needs to be investigated. Towards this, nanobubbles were imaged on PS films in DI water and saline solution using TMAFM. The model of charged structure for nanobubbles was further explored by studying the effect of pH as well as substrate bias.

2. Experimental

A commercial D3000 AFM with a Nanoscope IV controller (Bruker Instruments) operating in tapping mode (TMAFM) was used for all AFM imaging. For liquid imaging, a commercial fluid cell (DTFML-DD, Bruker Instruments) was used which had a piezo element dedicated to directly drive the cantilever in fluid. A schematic of the fluid cell is shown in Fig. 1(a). In previous work on imaging nanobubbles,[30] a commercial Multimode III AFM (Bruker Instruments) with a modified tip holder was used. The design of dimension AFM allows the use of a larger volume of liquid compared to the Multimode, which is critical to the current work involving experimental liquid with dissolved solute. A larger volume helps to avoid fouling of the AFM tip caused by deposition of solute upon evaporation of the operating liquid.

Importantly, the polychlorotrifluoroethylene (PCTFE) casing which encloses the piezo in the DTFML fluid cell completely insulates it from liquid exposure. In contrast, the piezo of the modified tip holder[6] used with the Multimode AFM gets exposed to the operating liquid during imaging. This promoted electrolysis of the liquid, brought about by the drive amplitude voltage applied to the piezo electrodes during TMAFM imaging. Fig. 1 (b) shows the height images of nanobubbles on the same PS film in DI water imaged using the D3000 and the Multimode. The nanobubbles imaged with the D3000 were smaller than those imaged with the Multimode due to the pronounced electrolysis of DI water caused by the applied electric field in the latter.

A silicon nitride cantilever DNPS (Bruker Instruments) with a nominal tip radius <10 nm, a quoted stiffness of 0.35 N m^{-1}, and Ti/Au backside coating was used for liquid imaging. A silicon cantilever Multi75Al (BudgetSensors) with a nominal tip radius <10 nm, a quoted stiffness of 3 N m^{-1} and Al backside coating was used for imaging in air. The measured resonance frequency of the silicon cantilever was about 78 kHz in air. For the silicon nitride cantilever two prominent peaks for the resonance frequency were measured at about 14 and 19 kHz in the experimental liquids. For imaging in both air and liquid, drive frequencies were chosen close to the resonance frequency of the cantilever. A scan rate of 1 Hz with a scan angle of 0° was used for all imaging. The oscillation amplitude of the cantilever was set at 90% of the free amplitude to minimize the force on the

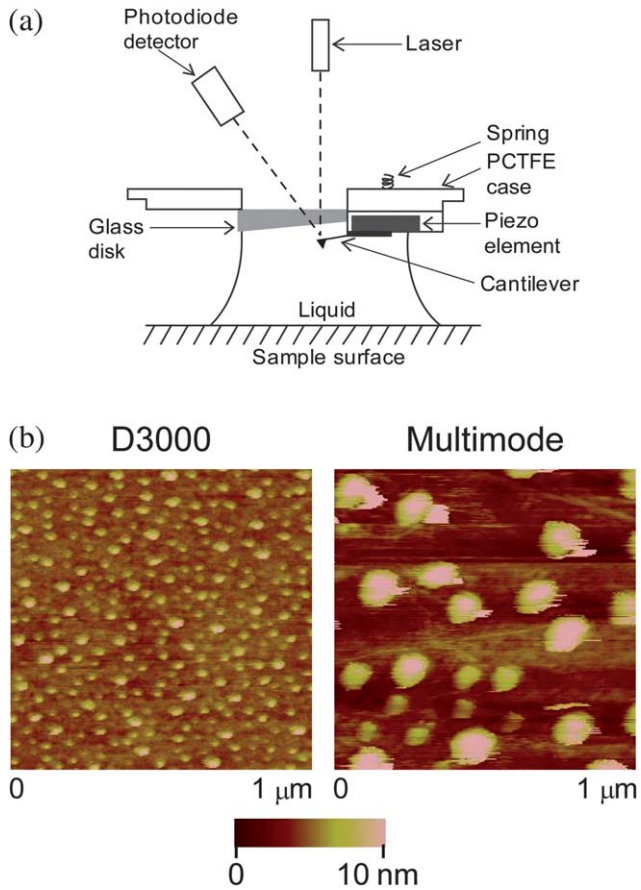

Fig. 1 (a) Schematic representation of a direct drive fluid cell for liquid imaging with the D3000 AFM, and (b) height images of nanobubbles formed on the PS film in DI water using the D3000 and the Multimode AFM. The piezo electrodes of the fluid cell in the Multimode AFM are exposed to liquid during imaging leading to the electrolysis effect causing formation of larger nanobubbles. In contrast, the piezo electrode in the fluid cell for the D3000 is insulated from liquid exposure by PCTFE casing thus preventing the electrolysis effect and hence causing formation of smaller nanobubbles.

nanobubbles and sample surface. All imaging experiments were performed in ambient environment (temperature: 20 ± 1 °C).

A PS sample was prepared by spin-coating an ultra-thin film of PS onto a Si (100) substrate at a speed of 2000 rpm. The substrate was cleaned by sonicating in acetone and then in isopropyl alcohol for 5 min each. The PS solution of concentration 1% (w/v) used for spin-coating was prepared by dissolving PS pellets (molecular weight 350 000, Sigma-Aldrich) in toluene (Mallinckrodt Chemical). To remove any remaining solvent, the PS sample was annealed in a convection oven at a temperature of 53 ± 2 °C for 4 hours. The contact angle of the resulting PS film with water was measured to be 93 ± 2° using a sessile drop method. The film thickness was measured to be 25 ± 5 nm with an ellipsometer (model L116C, Gaertner Scientific Corporation). The surface roughness was measured using an AFM in the tapping mode over a 5 μm × 5 μm scan area. For the effect of roughness study, samples were prepared at a speed of 500 rpm in order to obtain a more rough sample. Roughness and contact angle data are summarized in Table 1. The experimental liquids studied in this work were DI water and saline solution (Hospira) of concentration 0.9% (w/w).

To study the size distribution of nanobubbles, TMAFM was performed on the PS film immersed in DI water and saline solution. Past studies suggest that the propensity of formation and size of nanobubbles is affected by surface roughness and uniformity.[33] In the current work, care was taken to exclude the possibility of non-uniformity in surface roughness and film quality affecting the results from two different liquids. The roughness of a freshly prepared PS film was measured at multiple sites across the sample surface.

Subsequently, TMAFM imaging of the film immersed in DI water was performed at different sites across the sample surface with pristine film area, previously unexposed to liquid, being imaged each time. Repeatable size distribution of nanobubbles obtained from the images of each experiment confirmed the film-uniformity. A new PS sample was prepared and characterized in terms of surface roughness. The PS film was then immersed in DI water and imaged for nanobubbles. An unexposed part of the same sample surface was then immersed in saline solution and imaged with TMAFM to study and compare size distribution of nanobubbles in DI water and saline solution.

To study the effect of pH, DI water and saline solution each at three different pH values (3.4, 7.0 and 10.1) were used. The pH of each solution was measured using a pH meter (IQ Scientific, Silicon ISFET sensor). The pH of DI water and saline solution was measured to be 7.0 ± 0.1 each. The target pH of 3.4 ± 0.1 and 10.1 ± 0.1 was achieved by adding 0.01 M HCl and 0.01 M NaOH solutions respectively, dropwise using a micropipette to the experimental liquid (DI water or saline solution) of pH 7.0.

To study the effect of substrate bias, electrical bias was applied to the silicon substrate with respect to an electrode immersed in the liquid droplet on the PS surface. A DC power supply (Agilent E3612A, 0–120 V, 0–1.5 A) was used for the purpose. A liquid droplet was added on the PS film on Si substrate after biasing the substrate with positive or negative potential. The sample surface was then scanned for height images. The applied bias was increased up to 60 V in steps of 10 V and the height images were obtained at different locations at each step. During the experiments, each chosen voltage was continuously applied while the TMAFM imaging was performed. The height images were recorded at the same location as the previous step as well as at locations away from the previously scanned position. This allowed us to ensure that any effect observed is not from coalescence of the nanobubbles under the continuous scan load.

3. Results and discussion

In this section, TMAFM images of nanobubbles on a PS film immersed in DI water and saline solution are presented first. The histogram and geometrical distribution of nanobubbles deduced from AFM image analysis are then presented. The effect of surface roughness on the formation propensity and size distribution of nanobubbles is then explored. The results are analyzed in terms of the surface charge of nanobubbles. Morphological changes on the PS film due to liquid exposure for an extended period of time and 3D shape analysis of nanobubbles are presented. Finally the effect of pH and applied substrate bias on nanobubble characteristics is presented.

Table 1 Comparison of AFM roughness (over 5 μm × 5 μm area) and contact angle in different PS films on Si

Spin speed (rpm)	Film thickness (nm)	RMS roughness (nm)	*P–V* distance (nm)	Static contact angle (°)	Average diameter of nanobubbles formed in DI water (nm)	Average diameter of nanobubbles formed in saline (nm)
500	44 ± 3	0.64 ± 0.08	7.0 ± 2.0	92.8 ± 2	54	50
2000	25 ± 5	0.44 ± 0.06	5.4 ± 2.0	93.1 ± 2	23	29

3.1 Nanobubble size distribution

Fig. 2 shows the AFM images and the corresponding histogram of a PS surface immersed in DI water and saline solution, each at pH 7.0 ± 0.1. The same 1 μm × 1 μm area of the PS surface in the liquid was continuously scanned for 15 scan cycles. Results after 3 and 15 cycles are presented here. Nanobubbles are observed to form on PS in both DI water and saline solution covering the entire scanned area. Images after 3 (top row) and 15 (bottom row) scan cycles indicate that there is no significant coalescence of nanobubbles over time under the influence of scan load. It is also evident that larger nanobubbles form in saline solution compared to DI water. Histogram analysis of the AFM images shows that in both liquids there is a distribution in the size of the nanobubbles. However, the size distribution of nanobubbles in DI water has a broader peak than in saline solution. A quantitative estimate of the nanobubble distribution was obtained by analyzing the percentage area covered, the total count, and the average diameter after 3 and 15 cycles, as shown in Fig. 3. The area covered by the nanobubbles after 3 cycles is 10% and remains the same after 15 cycles. For saline solution, the area covered is 19% after 3 cycles and after 15 cycles remains constant within the experimental uncertainty. The percentage area covered by the nanobubbles in saline solution is thus roughly twice as much as in DI water. The total count of nanobubbles on the PS film in DI water and after 3 cycles is around 210 and is approximately 24% higher for saline solution where the total count is found to be around 260. There is no significant change in the total nanobubble count after 15 cycles in either of the experimental liquids. The average diameter of nanobubbles in DI water is on the order of 23 nm. In saline solution, the average diameter is relatively higher at around 28 nm. The average diameter of nanobubbles did not change between 3 and 15 cycles. The data also show that between 3 and 15 scan cycles, there is no measurable change in the distribution parameters indicating that there is no appreciable coalescence happening over the time period of the experiments.

In electrolytic solution, the Debye length κ is given by

$$1/\kappa = \sqrt{\frac{\varepsilon\varepsilon_0 k_B T}{2N_A e^2 I}} \quad (1)$$

where ε is the permittivity of free space, ε_0 is the dielectric constant or permittivity relative to free space, k_B is the Boltzmann constant, T is the absolute temperature in K, N_A is the Avogadro number, e is the elementary charge, and I is the ionic strength in mole m^{-3}.[16,23] Past studies indicate that nanobubbles are a charged species,[11,17] and negative charges preferentially reside at the air–water interface. Schematically, nanobubbles can be represented as shown in Fig. 4. To maintain the overall electrical neutrality of solution, a layer of positive charges accumulate surrounding the layer of negative charges thus forming an electrical double layer. In this case, the Debye length represents the thickness of the electrical double layer. The inter-nanobubble

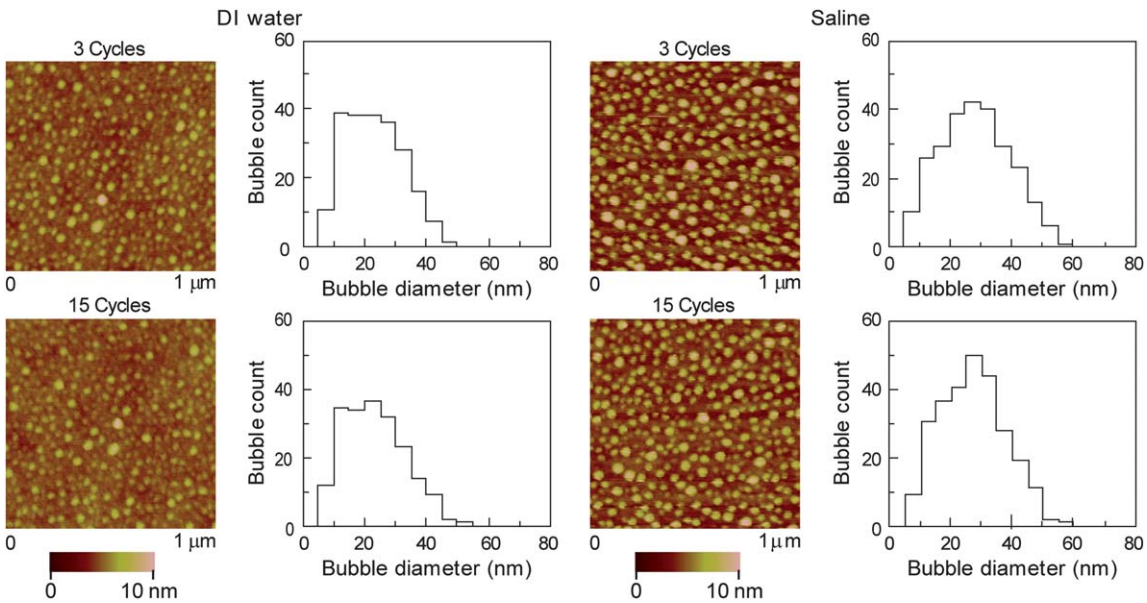

Fig. 2 Height images and the corresponding histogram of the size distribution of nanobubbles formed on the PS film in DI water and saline solution. Data presented after 3 and 15 scan cycles for each liquid. Number of nanobubbles is larger in saline solution compared to DI water.

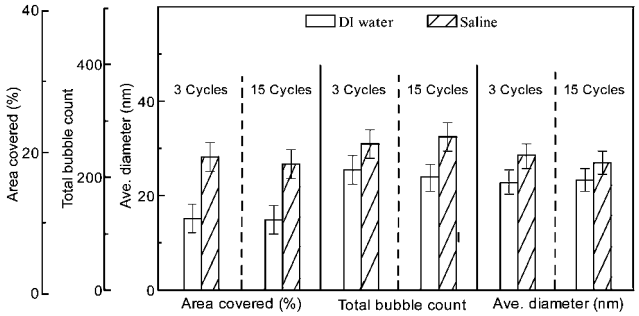

Fig. 3 Geometrical distribution of nanobubbles shown in Fig. 2. The area covered, total count, and average diameter of nanobubbles on the PS film in DI water and saline solution after 3 and 15 scan cycles. The percentage area covered, total count, and average diameter of nanobubbles are larger in saline solution compared to DI water.

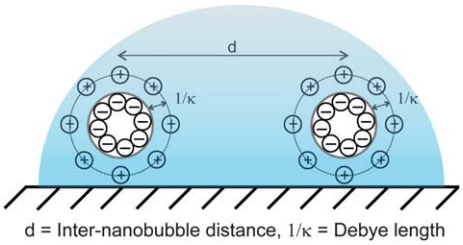

Fig. 4 Cartoon showing nanobubbles as charged species forming an electrical double layer. The electrostatic repulsion between two such adjacent charged structures determines the inter-nanobubble distance.

distance, defined by d, between two neighboring nanobubbles is determined by the electrostatic repulsion between the two charged structures and hence influences the stability of nanobubbles. There is an increased ionization in saline solution compared to DI water. Increased negative charges now reside at the nanobubble interface and form a strong electrical double layer (EDL). Electrostatic repulsion subsequently stabilizes the nanobubbles. This potentially leads to a larger number of nanobubbles in saline solution. The larger number of nanobubbles thus formed, when in close proximity, may coalesce to form relatively larger sized nanobubbles in saline compared to DI water.

3.2 Effect of surface roughness

Fig. 5 shows height images of nanobubbles on PS films of two different roughnesses each immersed in DI water and saline solution. Results are presented here after 3 and 15 cycles. The RMS roughness σ of the two PS films in air is 0.64 ± 0.08 nm and 0.44 ± 0.06 nm respectively. For both DI water and saline solution, larger nanobubbles formed on the PS film of higher roughness as observed in the height images after 3 cycles. These larger nanobubbles, formed on the PS film of higher roughness, readily coalesced over time under the influence of scan load. Hence, after 15 cycles (bottom row), there was an increase in the size of nanobubbles and a decrease in their number. This coalescence phenomenon was observed for both DI water and saline solution. The PS film of lower roughness resulted in the formation of nanobubbles which were small enough and remained unaffected by the scan load and did not coalesce over time.

The geometrical distribution of nanobubbles on the PS film of different roughnesses in DI water and saline solution is shown in Fig. 6. In DI water, the area covered by nanobubbles on the PS film of higher roughness is about 18% and that on a film of lower roughness is about 10% after 3 cycles. In saline solution, the area covered by nanobubbles on the PS film of higher roughness is about 20% and that on a film of lower roughness is about 17% after 3 cycles. For the PS film of higher and lower roughnesses, the average diameters of nanobubbles in DI water after 3 cycles are around 54 nm and 23 nm, respectively (Table 1). The average diameters of nanobubbles in saline solution after 3 cycles are around 50 nm and 29 nm for the PS film of higher and lower roughnesses, respectively (Table 1). It is evident that for DI water and saline solution, the average diameters of nanobubbles on the higher roughness film are 2.3 and 1.7 times larger, respectively, than that on the lower roughness film. Coalescence of nanobubbles is evident from the sharp decrease in total count and increase in average diameter of nanobubbles after 3 and 15 cycles. This trend is evident for both DI water and saline solution but coalescence is more pronounced in the case of saline solution compared to DI water.

Roughness can promote formation of nanobubbles due to concave areas which are unfavorable for water to penetrate resulting in a gas cavity and nanobubbles with lower curvature and greater stability. It is believed that the influence of film roughness on nanobubble size and count is related to the larger number of nanobubble formation sites on a rough surface.[33] Surface asperities of a rough film provide more nucleation sites for nanobubble formation. This is because the surface asperities prevent water from penetrating resulting in localized pockets of gas cavity. These gas cavities of nanobubbles are of lower curvature than the surface asperities and hence have high stability. Hence the formation of nanobubbles is favored. Further growth of the nanobubble seed at these numerous sites leads to coalescence and formation of larger nanobubbles. The film with higher roughness thus causes formation of relatively larger nanobubbles than that with lower roughness.

3.3 Shape of nanobubbles

Nanobubbles are mostly found to be spherical cap-shaped structures.[9,37] Less commonly, researchers have also reported flat gaseous layers called micro and nanopancakes, either isolated or in conjunction with nanobubbles, forming on HOPG in water and saline solution.[13,24] The shapes of these nanopancakes are reportedly influenced by the cleavage steps of the HOPG surface. Another interesting observation[39] is that interfacial gas could form one or more layers on top of a flat gas layer leading to bilayers and tri-layers of gaseous structures on the solid surface. These gaseous structures, formed due to local gas supersaturation, were observed to transform to nanobubbles under the influence of tip perturbation.

In our case 3D shape analysis shows that nanobubbles are mostly spherical cap-shaped structures as evident from the left image in Fig. 7. However, larger nanobubbles of average diameter around 50 nm and higher which formed on the PS film of

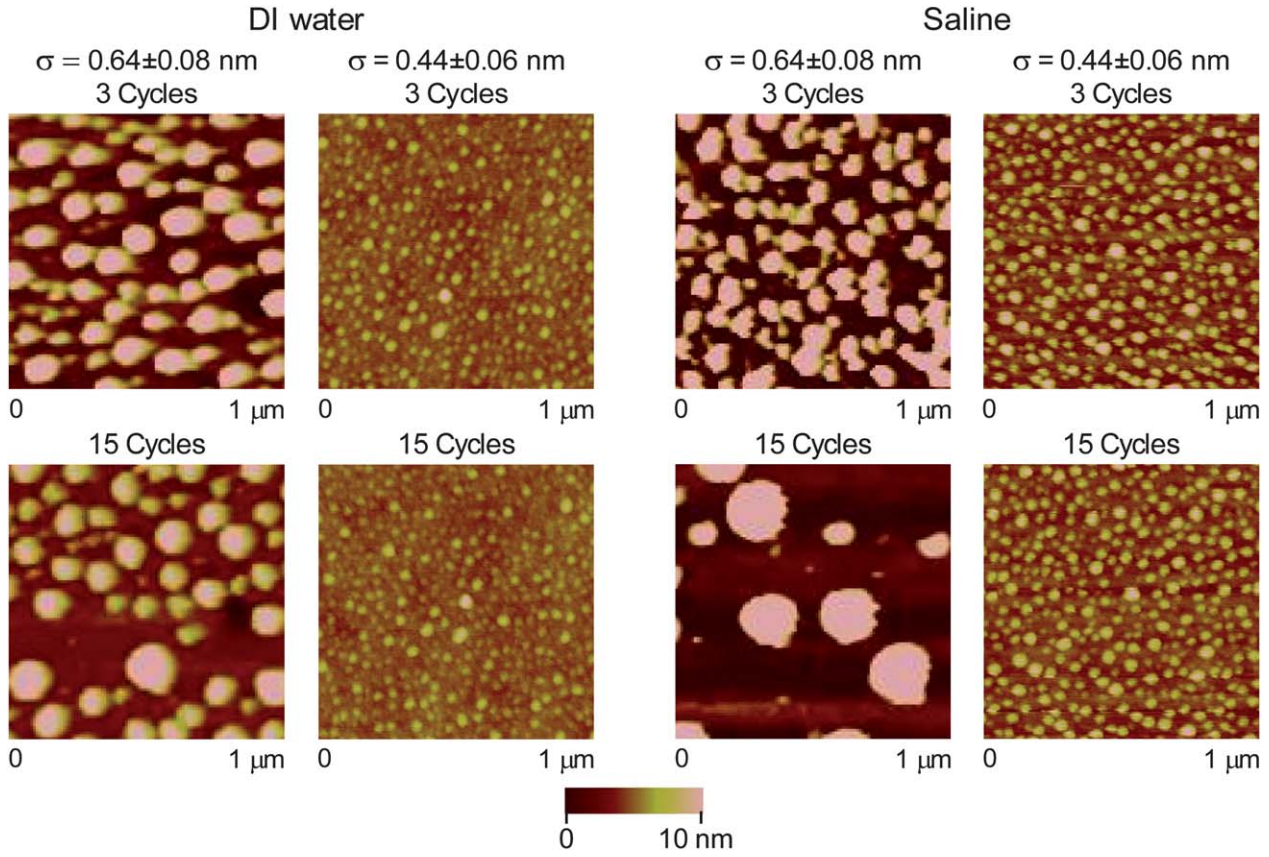

Fig. 5 Height images of nanobubbles on PS films of two different σ roughnesses. Data presented for nanobubbles in DI water and saline solution after 3 and 15 scan cycles. Film with higher roughness and hence more nucleation sites causes formation of relatively larger nanobubbles than that with lower roughness. These larger nanobubbles, formed on the PS film of higher roughness, readily coalesce over time under the influence of scan load.

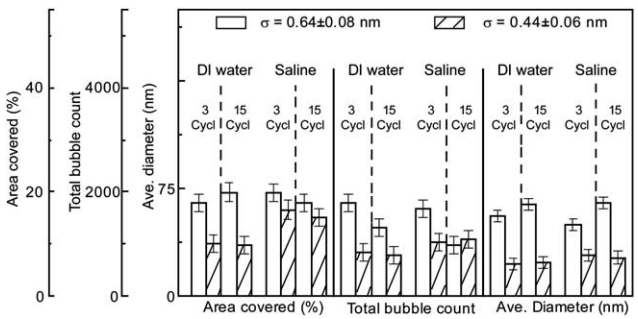

Fig. 6 Geometrical distribution of nanobubbles shown in Fig. 5. The area covered, total count and average diameter of nanobubbles on the PS film, of two different RMS roughnesses, in DI water and saline solution after 3 and 15 scan cycles. The percentage area covered by nanobubbles is larger on film with higher roughness. Nanobubble coalescence under the AFM tip scan load after 15 scan cycles is evident from sharp decrease in total bubble count and increase in average bubble diameter.

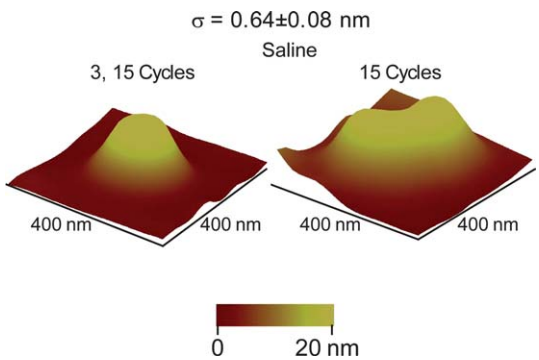

Fig. 7 3D shape analysis of nanobubbles formed on the PS film in saline solution. Nanobubbles are mostly spherical cap-shaped structures. However coalescence under the scan load of an AFM tip may lead to pancake-shaped structures.

higher roughness were more prone to coalesce when subjected to tip scan load for prolonged time. As shown in the right image in Fig. 7, larger and flattened gas structures may result through coalescence. This is in contrast to previous reports where flatter nanopancakes are observed in the initial phase of imaging with an AFM tip.

3.4 Liquid exposure effects on topography

Fig. 8 shows the height images of the PS film in air before and after exposure to liquid at the end of 360 min. The top row shows images of the PS film of lower roughness $\sigma = 0.44 \pm 0.06$ nm while the bottom row shows images of the PS film of higher roughness $\sigma = 0.64 \pm 0.08$ nm. The leftmost images show the height images of pristine featureless PS film. After exposure to

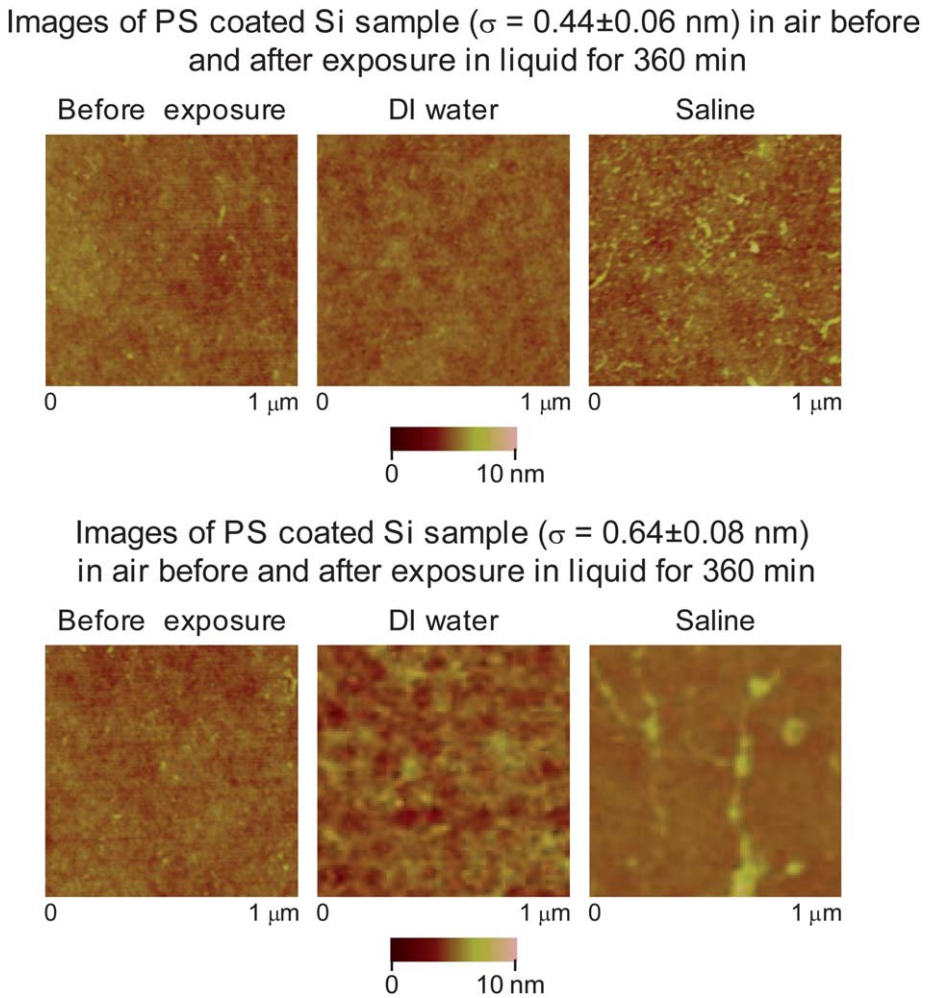

Fig. 8 Effect of liquid exposure on the film topography. Height images of the PS film in air before and after exposure to DI water and saline solution at the end of 15 scan cycles. The PS film of higher roughness (larger nanobubbles formed) shows nanoindents when imaged in air at the end of 360 min of exposure to DI water.

saline solution, both the PS films show extensive solute deposits on the surface. Interestingly, the PS film of higher roughness (bottom row) when exposed to DI water (larger nanobubbles formed) shows nanoindents when imaged in air at the end of 360 min of exposure to DI water. A point to note here is that this film of higher roughness resulted in the formation of larger nanobubbles with greater internal pressure. This leads to the formation of nanoindents.[31]

3.5 Effect of pH

The surface charge characteristic of nanobubbles is further explored by studying the effect of pH on the size distribution of nanobubbles on the PS film in DI water and saline solution. Fig. 9 shows the height images and the corresponding histogram of nanobubbles in DI water (left two columns) and saline solution (right two columns) at pH 3.4, 7.0, and 10.1. The results show that as the pH increases from 3.4 to 10.1, the nanobubbles become larger in size. The trend is similar for both DI water and saline solution. In the case of saline solution, the increase in the size of nanobubbles is more pronounced between pH 7.0 and 10.1 than between 3.4 and 7.0.

Fig. 10 shows the geometrical distribution of nanobubbles on the PS film immersed in DI water and saline solution at the three different pH values. The area covered by nanobubbles in DI water is around 7%, 22%, and 24% of the total surface area scanned at pH 3.4, 7.0, and 10.1 respectively. For saline solution, the area covered by nanobubbles is 17%, 27% and 30% of the total surface area at the above mentioned three pH values. The total count of nanobubbles in DI water in the pH range 3.4–10.1 remains mostly around 180. On the other hand, in the above pH range, the total count of nanobubbles in saline solution increases from around 200 to 225. The average diameter of nanobubbles is observed to increase markedly from 21 nm to 37 nm in DI water and from 30 nm to 38 nm in saline solution as the pH is increased from 3.4 to 7.0. This means more than 75% and about 27% increase in the size of nanobubbles for DI water and saline solution, respectively, as the pH is increased from acidic to neutral range. This indicates that nanobubbles are unstable in acidic solution. In the alkaline pH, the average diameter increases to 39 nm in DI water and to 48 nm in saline solution. In

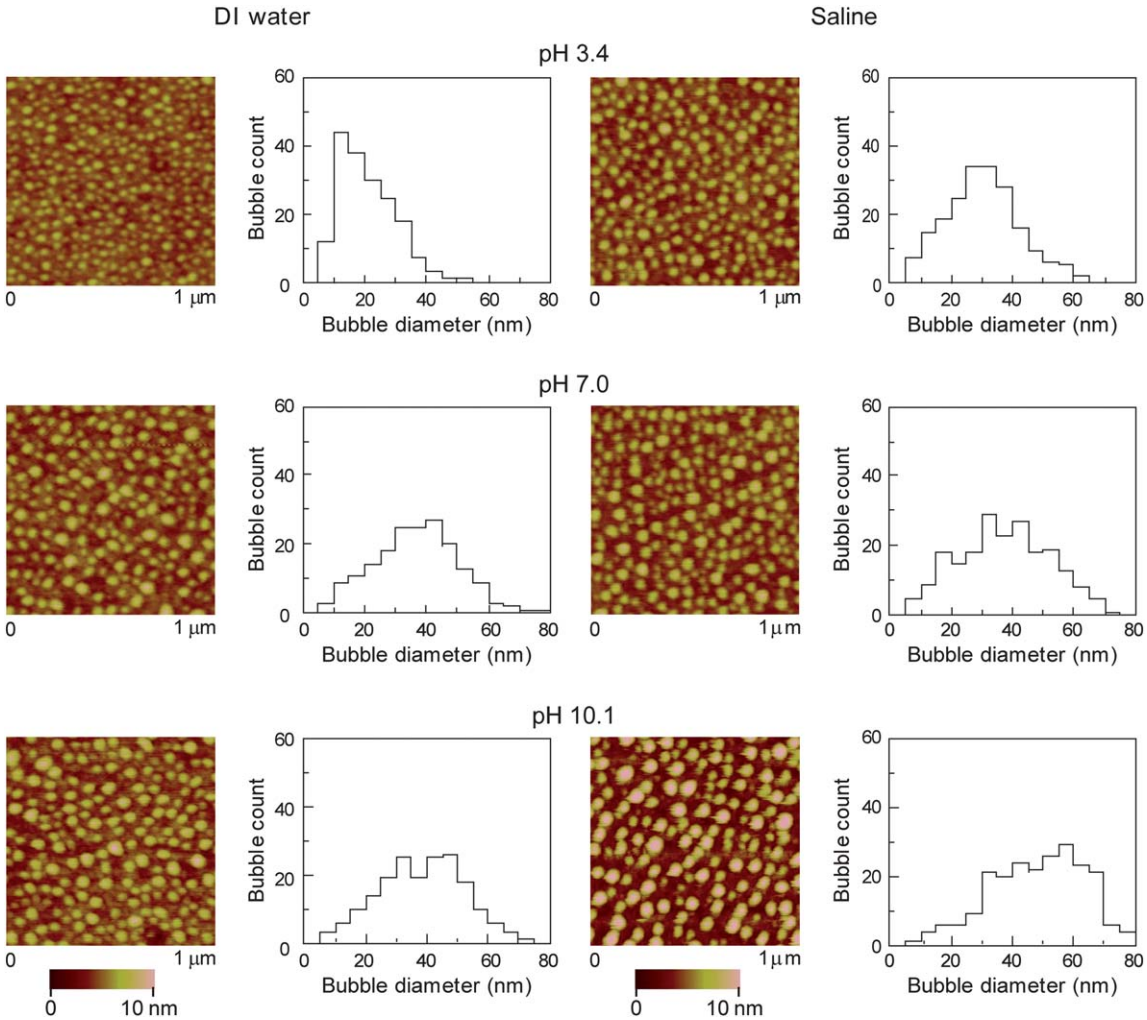

Fig. 9 Effect of pH on the size distribution of nanobubbles on the PS film in DI water and saline solution illustrated by height images and histogram analysis at pH 3.4, 7.0, and 10.1. The size of nanobubbles becomes larger at higher pH than at lower pH.

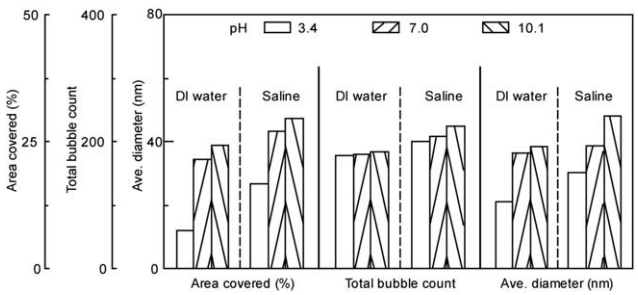

Fig. 10 Geometrical distribution of nanobubbles shown in Fig. 9. The area covered, total count and average diameter of nanobubbles on the PS film in DI water and saline solution are shown at pH 3.4, 7.0 and 10.1. The percentage area covered, total count and average diameter of nanobubbles show an increasing trend with increase in pH.

summary, the percentage area covered, total count, and average diameter of nanobubbles each show an increasing trend with increase in pH. The above results suggest that for a given ionic strength, nanobubbles are more stable as the pH is increased from acidic to alkaline range.

The above trend can be attributed to the differential stabilization of the nanobubbles on the surface of the PS film by different charged species present in the solution at different pH values. Past studies suggest that a macroscopic gas/water interface without any solute is negatively charged because the hydroxyl ions (OH^-) from the dissociation–association of water molecules prefer to stay at the gas–water interface.[17,22] The H^+ ions preferentially stay in the bulk aqueous phase allowing OH^- to reside at the gas–water interface—an effect referred to as "negative adsorption" or "proton exclusion".[22] In the acidic range, the increase of proton concentration not only increases the ionic strength and reduces the thickness of the electric double layer but also neutralizes the negatively charged gas/water interface and destabilizes the nanobubbles. It is worthwhile to note that the addition of NaOH to adjust pH has two opposing effects on the formation of stable nanobubbles. On one hand, adsorption of more OH^- ions increases negative charges at the gas/water interface and enhances the electrical double layer and hence stabilizes the nanobubbles. On the other hand, it increases the ionic strength of the solution and reduces the effective interbubble repulsive force so that the nanobubbles can undergo

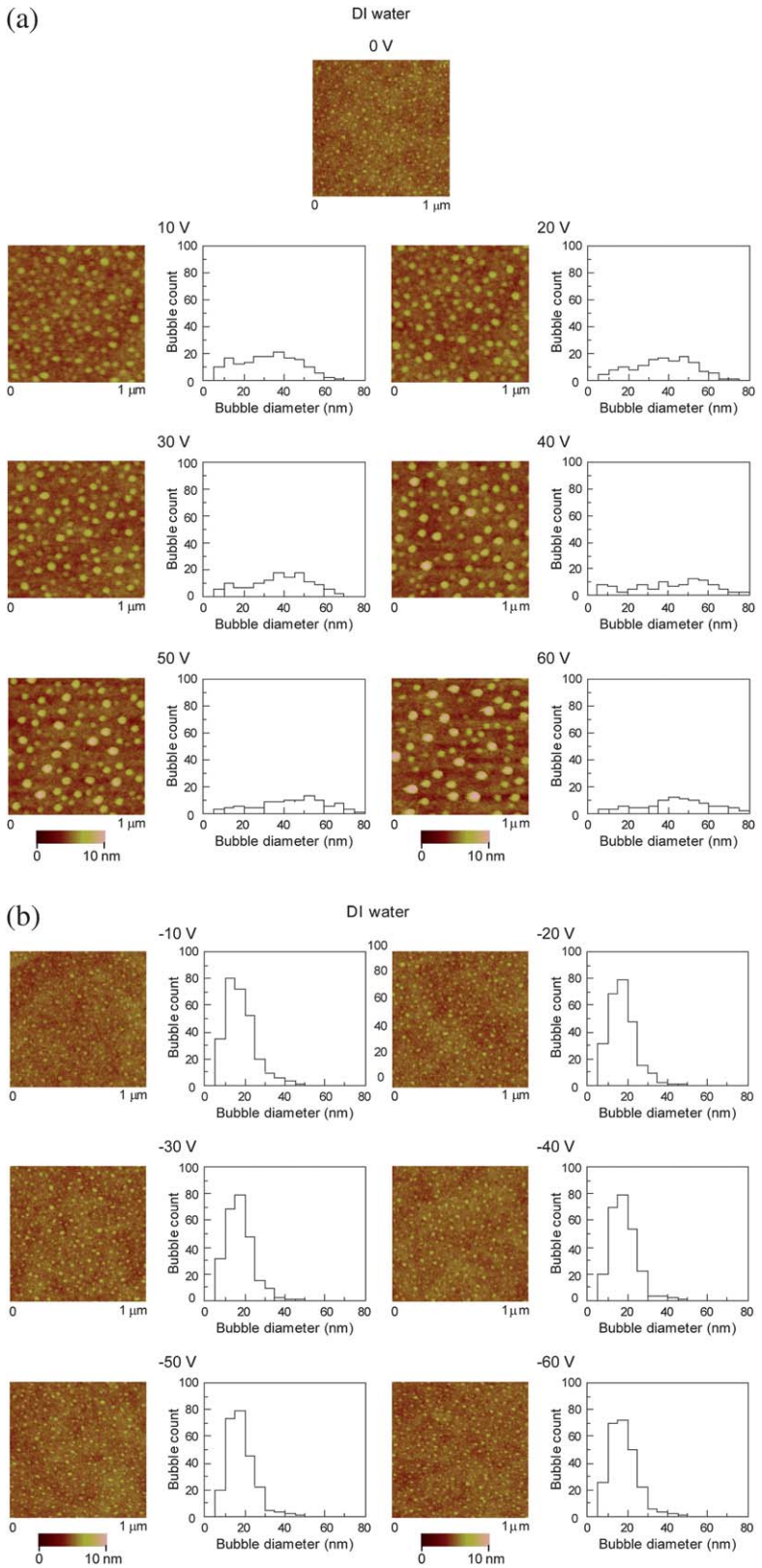

Fig. 11 (a) Height images and the corresponding histogram of the size distribution of nanobubbles on the PS film in DI water for a series of positive potential applied to the silicon substrate with respect to the liquid, and (b) height images and the corresponding histogram of the size distribution of nanobubbles on the PS film in DI water for a series of negative potential applied to the silicon substrate with respect to the liquid.

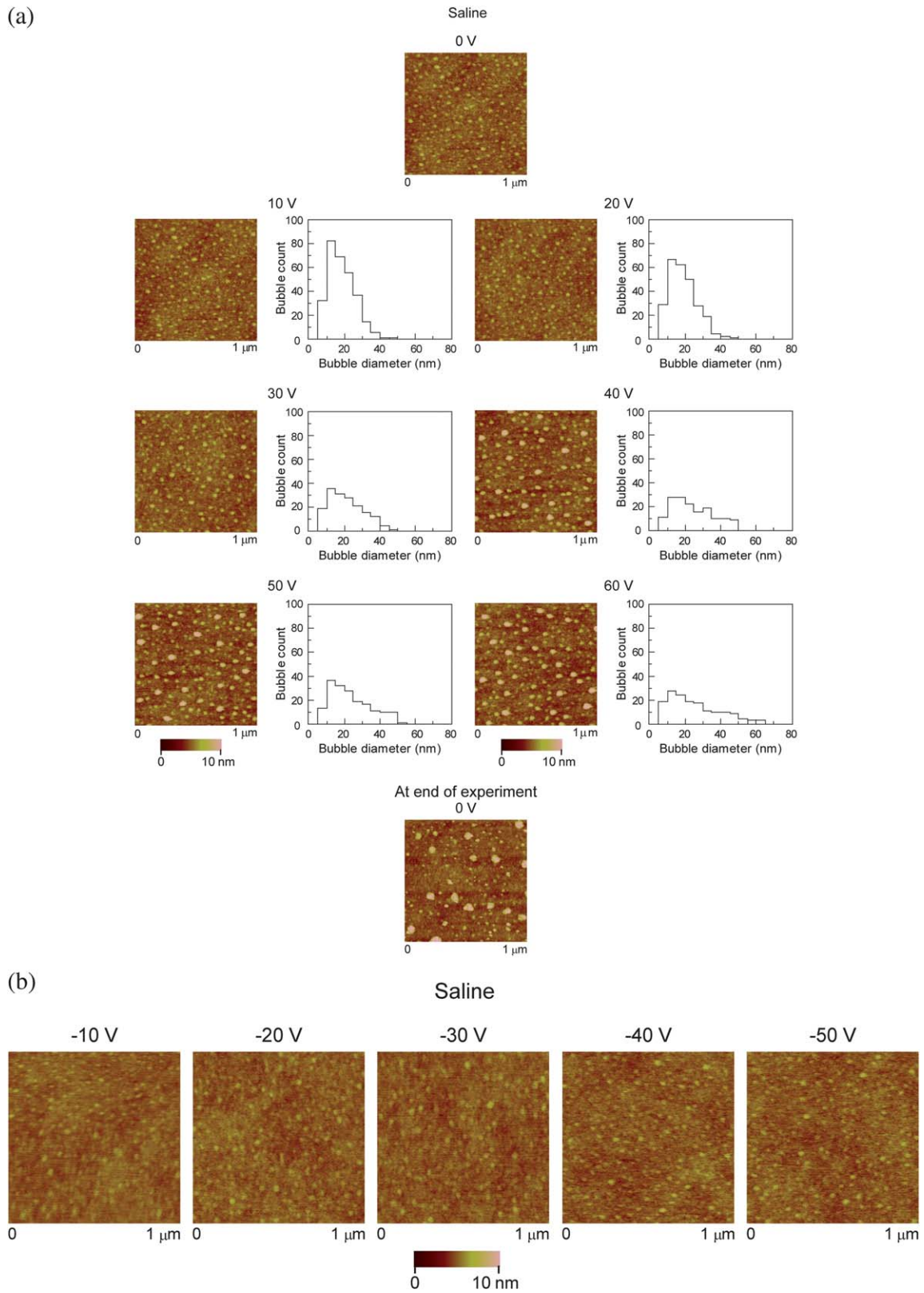

Fig. 12 (a) Height images and the corresponding histogram of the size distribution of nanobubbles on the PS film in saline solution for a series of positive bias applied to the silicon substrate. The top and the bottom row show the height images of nanobubbles in saline solution without substrate bias before and after the experiment with positive potential. (b) Height images of nanobubbles on the PS film in saline solution for a series of negative potential applied to the silicon substrate.

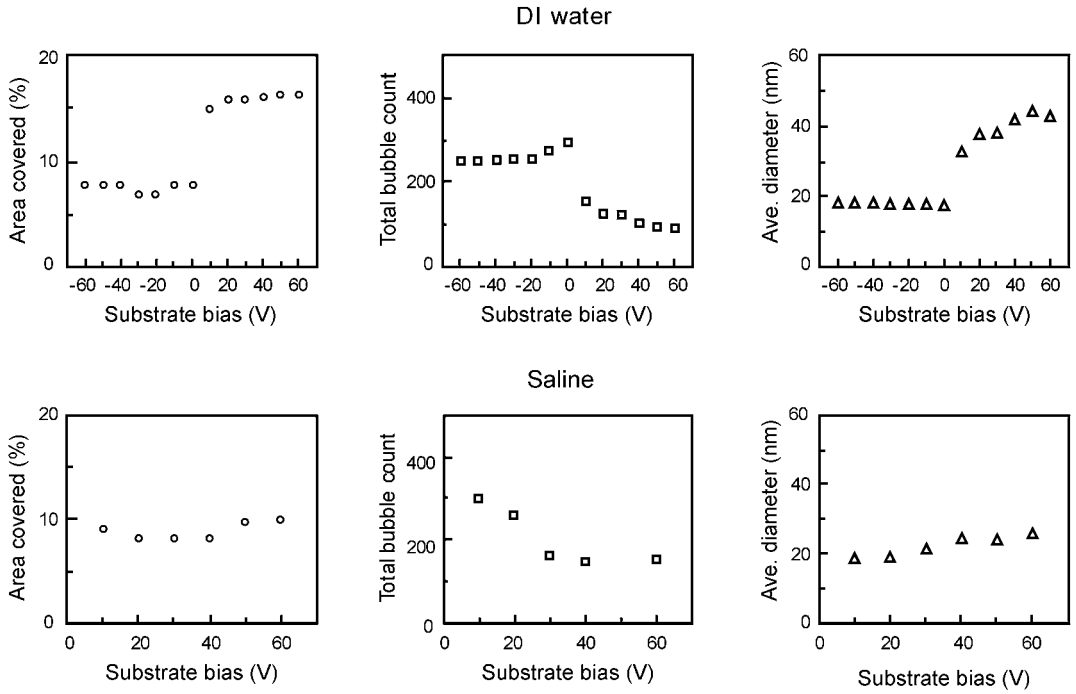

Fig. 13 Geometrical distribution of nanobubbles on the PS film in DI water (top row) and saline solution (bottom row) shown in Fig. 11 and 12, respectively. In DI water, the area covered and average diameter of nanobubbles increase and the total count of nanobubbles decreases with increasing positive potential applied to the silicon substrate. The distribution of nanobubbles is relatively unaffected in the range of negative potential. Similarly, in the case of saline solution the area covered and average diameter of nanobubbles increase and the total count of nanobubbles decreases with increasing positive potential applied to the silicon substrate.

aggregation and coalescence. Our results reveal that adsorption of more OH^- ions is dominant, so that for a given ionic strength, the nanobubbles are much more stable as the pH is increased from acidic to alkaline range.

3.6 Effect of substrate bias on nanobubbles

Fig. 11(a) shows the height images of nanobubbles on the PS film immersed in DI water with an electrical bias in the range of 0 V to 60 V applied to the silicon substrate. Histogram analysis of the images is also shown in the range 10 V to 60 V. Fig. 11(b) shows height images of nanobubbles on the PS film immersed in DI water with an electrical bias in the range −10 V to −60 V applied to the substrate. When an increasing positive bias is applied to the silicon substrate the percentage area covered and the average diameter of nanobubbles increase, and the total count of nanobubbles decreases. However, the distribution of nanobubbles is largely unaffected on application of increasingly negative substrate bias. A similar trend on the size distribution of nanobubbles on the PS film in saline solution is observed when an electrical bias is applied to the substrate as evident from Fig. 12 (a) and (b). Fig. 12(a) shows the height images of nanobubbles on the PS film immersed in saline solution with an electrical bias in the range 0 V to 60 V applied to the silicon substrate. The bottom row of Fig. 12(a) also shows the height image of nanobubbles on the same PS film in saline solution after the external power supply is removed at the end of the series of measurements. Furthermore, the histogram analysis of the height images in the range 10 V to 60 V is also shown here. The size of the nanobubbles is observed to increase as the substrate bias is increased. Interestingly, the size of nanobubbles imaged after removal of the external power supply is larger than that at a substrate bias of 60 V. The height images of nanobubbles on the PS film in saline solution at substrate bias in the range −10 V to −50 V are shown in Fig. 12(b). No appreciable change in the size of nanobubbles is observed with increasing negative substrate bias.

A quantitative estimate of the percentage area covered, the total count, and the average diameter of nanobubbles as a function of applied substrate bias is shown in Fig. 13 for DI water (top row) and saline solution (bottom row). For DI water, the area covered by nanobubbles increases from about 8% to 16% of the total surface area or a two-fold increase of area coverage in the range 0 V to 60 V of substrate bias. The total count decreases from about 300 to 92 while the average diameter increases from around 18 nm to 44 nm in the above range of substrate bias. An almost 2.5 times increase in average diameter of nanobubbles clearly reveals the critical role of substrate bias on nanobubble size distribution. For saline solution, the area covered by nanobubbles varies in the short range of 9–10% in the range 10 V to 60 V of substrate bias. The total count sharply decreases from about 300 to 150 while the average diameter increases from around 18 nm to 25 nm in the above range of substrate bias. The geometrical distribution for saline solution is not shown in the negative range of substrate bias due to no appreciable change in the value of the parameters.

Asymmetric interface charge distribution under positive and negative bias affecting the overall electrical properties has been

reported in the case of multilayer heterostructures.[28] The impact of bias polarity on charging/discharging processes of the dielectric film[35] and the reduced effective bias due to charging across the dielectric film causing different stiction characteristics in micro-electromechanical system (MEMS) switches[36] has also been reported. In the present work, the limited effect seen when the substrate was negatively biased could possibly be attributed to the following. Due to the presence of the insulating silicon oxide and PS layers, there forms a gradient of differential charging across the insulating layers. The extent of charging across the two insulating layers varies depending on whether the substrate is positively or negatively biased. This is possibly caused by the interfacial charges at the substrate/oxide, oxide/PS, PS/liquid interfaces. We conjecture that differential charging occurs at the above interfaces causing a difference in the effective net bias at the PS/water surface even when the bias applied by the external power supply remains the same. This effective net bias is significantly small when the substrate is negatively biased with respect to the electrode in the liquid. The concept of reduced effective bias is further supported by the fact that when the external power supply is removed from the circuit at the end of the experiment with 60 V, as shown in the bottom row of Fig. 12 (a), the height images show nanobubbles which are significantly larger than those at 60 V. This can possibly be attributed to the fact that upon removal of the external power supply, the opposing effect on the net applied bias was removed.

ζ-Potential measurements conducted on the polystyrene film immersed in liquid with nanobubbles populating the surface could be the subject of future research. This could give interesting insight into quantitative correlation between the surface charge and population density of nanobubbles forming at the surface.

4. Conclusion

The study explored the various factors influencing the mechanism of formation and stability of surface nanobubbles. A systematic study of nanobubbles using tapping mode AFM imaging was carried out to understand the different factors affecting the mechanism of formation propensity and size distribution of nanobubbles in DI water and saline solution. The results show that nanobubbles of larger size and number form on the PS film in saline solution compared to DI water. Electrolyte ions in saline solution are likely to be the surface-charge stabilizing agent for nanobubbles and lead to formation of nanobubbles of larger size and number. Surface roughness also plays a critical role on the size distribution of nanobubbles. Films of higher rms roughness cause formation of larger nanobubbles than films of lower roughness. Surface asperities on a rough film provide more nucleation sites to nanobubbles which, when in close proximity, then coalesce to form larger nanobubbles. In general, nanobubbles are spherical cap-shaped structures. However, through coalescence, they may form flattened gas structures.

Since nanobubbles are a charged species with an electrical double layered structure, the pH of solution is crucial for the stability of nanobubbles forming on a film immersed in liquid. The results show that for a given ionic strength, nanobubbles are more stable, and their size increases as the pH is increased from acidic to alkaline range due to the increased charge stabilization of nanobubbles. The size distribution of nanobubbles on the PS film immersed in liquid is also affected by the electrical bias applied to the underlying substrate.

The study reveals that a positive substrate bias results in an increase in the size of nanobubbles for both DI water and saline solution whereas the negative substrate bias shows no measurable change in the size distribution of nanobubbles on the film immersed in the two experimental liquids. This is attributed to the differential charging at the interfaces of the insulating PS film causing an attenuation of the applied substrate bias and hence a subdued effect showing no measurable change in the size of nanobubbles.

This study thus advances the understanding of the role of surface charge on the formation and stability of nanobubbles and the interplay of various factors affecting their formation mechanism and distribution with potential applications in micro/nanofluidics.

Acknowledgements

The authors acknowledge the financial support from Revalesio Corporation, Tacoma, Washington (Sean German, program monitor). The authors also thank Dr Abdelhamid Maali for scientific discussions.

References

1 A. Agrawal, J. Park, D. Y. Ryu, P. T. Hammond, T. P. Russell and G. H. McKinley, Controlling the location and spatial extent of nanobubbles using hydrophobically nanopatterned surfaces, *Nano Lett.*, 2005, **5**, 1751–1756.
2 P. Attard, Nanobubbles and the hydrophobic attraction, *Adv. Colloid Interface Sci.*, 2003, **104**, 75–91.
3 P. Attard, M. P. Moody and J. W. G. Tyrrell, Nanobubbles: the big picture, *Phys. A*, 2002, **314**, 696–705.
4 P. Ball, Chemical physics: how to keep dry in water, *Nature*, 2003, **423**, 25–26.
5 B. Bhushan, *Springer Handbook of Nanotechnology*, Springer, Heidelberg, 3rd edn, 2010.
6 B. Bhushan, *Nanotribology and Nanomechanics I—Measurement Techniques and Nanomechanics, II—Nanotribology, Biomimetics, and Industrial Applications*, Springer-Verlag, Heidelberg, 3rd edn, 2011.
7 B. Bhushan, Y. Wang and A. Maali, Coalescence and movement of nanobubbles studied with tapping mode AFM and tip-bubble interaction analysis, *J. Phys.: Condens. Matter*, 2008, **20**, Art. # 485004.
8 B. Bhushan, Y. Wang and A. Maali, Boundary slip study on hydrophilic, hydrophobic and superhydrophobic surfaces with dynamic atomic force microscopy, *Langmuir*, 2009, **25**, 8117–8121.
9 B. M. Borkent, S. de Beer, F. Mugele and D. Lohse, On the shape of surface nanobubbles, *Langmuir*, 2010, **26**, 260–268.
10 A. Checco, T. Hofmann, E. DiMasi, C. T. Black and B. M. Ocko, Morphology of air nanobubbles trapped at hydrophobic nanopatterned surfaces, *Nano Lett.*, 2010, **10**, 1354–1358.
11 V. S. J. Craig, B. W. Ninham and R. M. Pashley, The effect of electrolytes on bubble coalescence in water, *J. Phys. Chem.*, 1993, **97**, 10192–10197.
12 S. Granick, Y. Zhu and H. Lee, Slippery questions about complex fluids flowing past solids, *Nat. Mater.*, 2003, **2**, 221–227.
13 M. A. Hampton and A. V. Nguyen, Accumulation of dissolved gases at hydrophobic surfaces in water and sodium chloride solutions: implications for coal flotation, *Miner. Eng.*, 2009, **22**, 786–792.
14 M. A. Hampton and A. V. Nguyen, Nanobubbles and the nanobubble bridging capillary force, *Adv. Colloid Interface Sci.*, 2010, **154**, 30–55.
15 M. Holmberg, A. Kuhle, J. Garnaes, K. A. Morch and A. Boisen, Nanobubble trouble on gold surfaces, *Langmuir*, 2003, **19**, 10510–10513.

16 J. Israelachvili, *Intermolecular & Surface Forces*, Academic, London, 3rd edn, 1992.
17 F. Jin, J. Li, X. Ye and C. Wu, Effects of pH and ionic strength on the stability of nanobubbles in aqueous solutions of α-cyclodextrin, *J. Phys. Chem. B*, 2007, **111**, 11745–11749.
18 K. Kikuchi, Y. Tanaka, Y. Saihara, M. Maeda, M. Kawamura and Z. Ogumi, Concentration of hydrogen nanobubbles in electrolyzed water, *J. Colloid Interface Sci.*, 2006, **298**, 914–919.
19 D. Lohse, Bubble puzzles, *Phys. Today*, 2003, **56**, 36–42.
20 K. G. Marinova, R. G. Alargova, N. D. Denkov, O. D. Velev, D. N. Petsev, I. B. Ivanov and R. P. Borwankar, Charging of oil–water interfaces due to spontaneous adsorption of hydroxyl ions, *Langmuir*, 1996, **12**, 2045–2051.
21 M. Mezger, H. Reichert, S. Schoder, J. Okasinski, H. Schroder, H. Dosch, D. Palms, J. Ralston and V. Honkimaki, High-resolution *in situ* X-ray study of the hydrophobic gap at the water–octadecyl–trichlorosilane interface, *Proc. Natl. Acad. Sci. U. S. A.*, 2006, **103**, 18401–18404.
22 A. S. Najafi, J. Drelich, A. Yeung, Z. Xu and J. Masliyah, A novel method of measuring electrophoretic mobility of gas bubbles, *J. Colloid Interface Sci.*, 2007, **308**, 344–350.
23 W. B. Russel, D. A. Saville, and W. R. Schowalter, *Colloidal Dispersions*, Cambridge University Press, 1989.
24 J. R. T. Seddon, E. S. Kooij, B. Poelsema, H. J. W. Zandvliet and D. Lohse, Surface bubble nucleation stability, *Phys. Rev. Lett.*, 2011, **106**, Art. # 056101.
25 R. Steitz, T. Gutberlet, T. Hauss, B. Klosgen, R. Krastev, S. Schemmel, A. C. Simonsen and G. H. Findenegg, Nanobubbles and their precursor layer at the interface of water against a hydrophobic substrate, *Langmuir*, 2003, **19**, 2409–2418.
26 M. Switkes and J. W. Ruberti, Rapid cryofixation/freeze fracture for the study of nanobubbles at solid–liquid interfaces, *Appl. Phys. Lett.*, 2004, **84**, 4759, 3pp.
27 M. Takahashi, ζ potential of microbubbles in aqueous solutions: electrical properties of the gas–water interface, *J. Phys. Chem. B*, 2005, **109**, 21858–21864.
28 V. M. Voora, T. Hofmann, M. Brandt, M. Lorenz, N. Ashkenov, M. Grundmann and M. Schubert, Electrical properties of ZnO–$BaTiO_3$–ZnO heterostructures with asymmetric interface charge distribution, *Appl. Phys. Lett.*, 2009, **95**, Art. # 082902.
29 V. Wallqvist, P. M. Claesson, A. Swerin, C. Ostlund, J. Schoelkopf and P. A. C. Gane, Influence of surface topography on adhesive and long-range capillary forces between hydrophobic surfaces in water, *Langmuir*, 2009, **25**, 9197–9207.
30 Y. Wang and B. Bhushan, Boundary slip and nanobubble study in micro/nanofluidics using atomic force microscopy, *Soft Matter*, 2010, **6**, 29–66.
31 Y. Wang, B. Bhushan and X. Zhao, Nanoindents produced by nanobubbles on ultrathin polystyrene films in water, *Nanotechnology*, 2009, **20**, Art. # 045301.
32 Y. Wang, B. Bhushan and X. Zhao, Improved nanobubble immobility induced by surface structures on hydrophobic surfaces, *Langmuir*, 2009, **25**, 9328–9336.
33 J. W. Yang, J. M. Duan, D. Fornasiero and J. Ralston, Very small bubble formation at the solid-water Interface, *J. Phys. Chem. B*, 2003, **107**, 6139–6147.
34 S. Yang, P. Tsai, E. S. Kooij, A. Prosperetti, H. J. W. Zandvliet and D. Lohse, Electrolytically generated nanobubbles on highly orientated pyrolytic graphite surfaces, *Langmuir*, 2009, **25**, 1466–1474.
35 U. Zaghloul, G. J. Papaioannou, H. Wang, B. Bhushan, F. Coccetti, P. Pons and R. Plana, Nanoscale characterization of the dielectric charging phenomenon in PECVD silicon nitride thin films with various interfacial structures based on Kelvin probe force microscopy, *Nanotechnology*, 2011, **22**, Art. # 205708.
36 U. Zaghloul, B. Bhushan, P. Pons, G. J. Papaioannou, F. Coccetti and R. Plana, Nanoscale characterization of different stiction mechanisms in electrostatically driven MEMS devices based on adhesion and friction measurements, *J. Colloid Interface Sci.*, 2011, **358**, 1–13.
37 X. H. Zhang, N. Maeda and V. S. J. Craig, Physical properties of nanobubbles on hydrophobic surfaces in water and aqueous solutions, *Langmuir*, 2006, **22**, 5025–5035.
38 X. H. Zhang, A. Quinn and W. A. Ducker, Nanobubbles at the interface between water and a hydrophobic solid, *Langmuir*, 2008, **24**, 4756–4764.
39 L. Zhang, X. Zhang, C. Fan, Y. Zhang and J. Hu, Nanoscale multiple gaseous layers on a hydrophobic surface, *Langmuir*, 2009, **25**, 8860–8864.

